JOURNAL OF CATALYSIS **171,** 169–176 (1997)
ARTICLE NO. CA971763

Model Pumices Supported Metal Catalysts

I. Preparation and Characterization of Supports and Supported-Palladium Catalysts

Leonarda F. Liotta,* Anna Maria Venezia,*,† Antonino Martorana,*,† Antonella Rossi,‡ and Giulio Deganello*,†

*Istituto di Chimica e Tecnologia dei Prodotti Naturali del CNR (ICTPN-CNR), via Ugo La Malfa 153, 90146 Palermo, Italy; and †Dipartimento di Chimica Inorganica, Università di Palermo, via Archirafi 26-28, 90123 Palermo, Italy; and ‡Dipartimento di Chimica e Tecnologie Inorganiche e Metallorganiche, Università di Cagliari, via Ospedale 72, 09124 Cagliari, Italy

Received February 10, 1997; revised April 21, 1997; accepted May 14, 1997

A series of aluminosilicates with similar silica/alumina ratios and similar structural properties of natural pumice, but with differing amounts of alkali ions in their framework, were prepared and characterized by different techniques such as IR, TG, physisorption, and XPS. The synthesis through the gel route yields quite homogeneous materials and, by varying the reaction mixture and the calcination parameters, allows one to obtain supports closely resembling the natural pumice. The corresponding palladium catalysts are prepared starting from two different precursors, $[Pd(NH_3)_4](NO_3)_2$ and $Pd(C_3H_5)_2$. The electronic properties, as obtained from photoelectron spectroscopy, and the structural parameters, obtained from X-ray diffraction techniques, are discussed in terms of the alkali ions/Pd atomic ratio and also in terms of the preparation methods.

INTRODUCTION

Pumice, a volcanic aluminosilicate, has recently been used as a support for palladium catalysts (1). Such catalysts exhibited good activity and selectivity in the liquid phase hydrogenation of 1,3-cyclooctadiene (2, 3) and phenylacetylene (4, 5) and in the gas phase hydrogenation of acetylene in ethylene rich feedstocks (6). The good catalytic performance was maintained even with high metal dispersion, differently from palladium catalysts supported on alumina (7–9), silica (9–11), and carbon (11, 12), showing a decline in activity above 20% metal dispersion.

The negative effect of a high metal dispersion in the hydrogenation of alkadienes (7, 8, 11–13) and alkynes (9, 10, 14, 15) over Pd/Al_2O_3, Pd/SiO_2, and Pd/C was attributed to the progressive loss of metallic character with decreasing particle size, as indicated (16, 17) by the positive Pd 3*d* binding energy shift with respect to unsupported palladium (7–15) in the XPS analyses. The electron deficiency character of the metallic centers would increase the strength of their interaction with the electron rich substrates, hindering the subsequent hydrogenation process. Recently (18), positive Pd 3*d* binding energy shifts were attributed to the morphology of the supported metal particles which, growing epitaxially on the α-alumina support, interact strongly with it. As a consequence the metal centers would be covered with the electron-rich substrate, obstructing the adsorption of hydrogen and favoring the isomerization reaction of the but-1-ene with respect to the hydrogenation reaction (19).

In contrast to the above findings, the XPS studies of pumice-supported palladium catalysts have detected a negative binding energy shift of the Pd 3*d* level. Such a shift was attributed to a metal–support interaction producing an increase in the electron density of the palladium particles (20, 21). The combination of the binding energy shifts with the Auger chemical shifts, yielding the Pd Auger parameters, allowed for the estimation of the electronic charge on the small palladium particles (22). The negative charge was found to increase with metal dispersion and also with the alkali metal ions/Pd atomic ratio (23). It was considered responsible for the enlarged range of applicability toward higher metal dispersion of these catalysts with respect to the palladium catalysts supported on alumina or silica. Similar negative binding energy shifts were observed in alkali ion-doped Pd/SiO_2 catalysts (24); however, the catalytic effects of the dopant ions appear different depending on whether they are added to the surface of the catalysts, as in the promoted Pd/silica catalysts, or they are present in the support framework, as in Pd/pumice catalysts. The different location of the promoter ions established by low-energy ion scattering (LEIS) analyses (25) accounts also for a different behavior in the adsorption of CO and CO_2 (26).

On the basis of the above results a series of amorphous aluminosilicates with variable Na^+, K^+, and $(Na^+ + K^+)$ contents and the relative palladium catalysts were prepared in order to study the effect of the support added alkali metal ions on the catalytic properties of these catalysts. The present article will describe the synthesis and the structural

0021-9517/97 $25.00

characterization of the supports and corresponding Pd catalysts. The catalytic performances in the hydrogenation of 1,3-cyclooctadiene will be reported in the subsequent paper (27).

EXPERIMENTAL

Materials

Supports. All operations were performed in standard Schlenk glassware under an atmosphere of prepurified nitrogen. Anhydrous alcohols (Aldrich) were obtained according to literature procedures (28) and distilled under nitrogen just before use. All other chemicals (Aldrich) were of reagent grade purity and used as received. All the supports with their chemical composition, their structural properties, and the thermal treatments are listed in Table 1. For comparison, the pumice and the precursor *gelsynt*$_0$ are also reported. The preparation of the supports was based on published procedures (29–31), modified to obtain the appropriate amorphous supports.

A typical preparation for the sodium containing supports, labeled in Table 1 with an *a*, is the following: a solution of Al(O-*sec*-Bu)$_3$ in anhydrous *sec*-butanol (100 ml) and a solution of MeONa in 10 ml anhydrous methanol were added to a stirred solution of Si(OEt)$_4$ in anhydrous ethanol (100 ml). The relative amounts of the three alkoxides were accordingly to the desired composition $SiO_2/Al_2O_3/Na_2O$ (see Table 1). The hydrolysis was performed by adding immediately water, in a fivefold excess of the required stoichiometric amount, to the rapidly stirred reaction mixture. The solution was then treated at 353 K for 3 h under N_2 flow. Upon cooling, a transparent, homogeneous, and colorless gel was obtained, which was filtered off under reduced pressure and washed with *sec*-butanol and ethanol to remove possible traces of alkoxides not hydrolyzed until washing fractions were completely clear on water addition. The xerogel was then calcinated, in air, at different temperatures, between 973 and 1223 K (see Table 1 for details on temperatures and time of calcination). After a rapid cooling to 293 K the product was crushed and sieved in various fractions. Only the powders of 40–70 mesh were collected and used for the preparation of the catalysts.

The precursor xerogel of *synt*$_0$ was divided into two portions: one was calcined at 973 K and yielded the amorphous *synt*$_0$; the other was treated with a solution of MeONa in CH_3OH/H_2O, at 298 K for 3 h, and, following the above procedure, was calcined at 1273 K to give the support Na-*synt*, which showed some crystallinity.

The potassium containing supports were prepared with the same procedure, using MeOK, except that only a 10% excess of water with respect to the required stoichiometric amount was used. Such catalysts are labeled in Table 1 with a *b*. The precursor gels were divided into two portions which were thermally treated differently, yielding the supports of type *b*1 and type *b*2.

Catalysts. Palladium catalysts were prepared with two different procedures; by ion exchange (32–34) and by an organometallic precursor (35).

The first method consisted of the following steps: $[Pd(NH_3)_4](NO_3)_2$, in aqueous solution, was passed through an ionic exchange resin (Amberlite IRA 100 regenerated in KOH, 0.5 *N*) to form $[Pd(NH_3)_4](OH)_2$ and dropped in a previously stirred (2 h) suspension of the synthetic pumice support in NH_3 saturated aqueous solution,

TABLE 1

Chemical Composition, Calcination Procedure, Specific Surface Area, and Specific Pore Volume of Natural Pumice, Precursor *Gelsynt*$_1$, and Synthetic Supports

Support	Density (g/cm^3)	SiO_2	Al_2O_3	Na_2O	K_2O	H_2O[a]	Heating rate (°C/min)	T_{max} (K)	BET (m^2/g)	Sp. pore vol. (cm^3/g)
Pumice	2.3	85.5	6.8	2.0	3.2	2.5				
Gelsynt$_0$	1.4	84.1	14.4			1.5			40	0.6
Synt$_0$ (*a*)	2.4	84.3	14.4			1.3	8	973	81	0.4
Synt$_{Na_1}$ (*a*)	2.4	83.5	14.3	0.6		1.5	8	1073	43	0.4
Synt$_{Na_2}$ (*a*)	2.4	83.4	14.2	1.4		0.9	8	1273	12	0.05
Synt$_{Na_3}$ (*a*)	2.4	81.1	13.9	4.0		0.9	8	1273	10	0.05
Synt$_{Na_4}$ (*a*)	2.4	79.9	13.6	5.6		0.9	8	1273	11	0.06
Na-synt (*a*)[b]	2.4	82.6	14.1	1.4		1.9	8	1273	14	0.05
Synt$_{Na\text{-}K_1}$ (*b*1)	2.0	83.1	14.2	0.6	0.7	1.4	1.7	973	162	0.6
Synt$_{Na\text{-}K_1}$ (*b*2)	2.3	83.5	14.3	0.6	0.7	0.9	0.3	1173	13	0.15
Synt$_{Na\text{-}K_2}$ (*b*1)	2.0	80.9	13.9	1.7	2.1	1.4	1.7	973	169	0.7
Synt$_{Na\text{-}K_2}$ (*b*2)	2.3	81.3	14.0	1.7	2.1	0.9	0.3	1173	11	0.05
Synt$_K$ (*b*1)	2.0	80.0	13.6		5.1	1.4	1.7	973	106	0.6
Synt$_K$ (*b*2)	2.3	80.2	13.8		5.1	0.9	0.3	1173	15	0.1

[a] Determined by thermogravimetric analysis.
[b] Synthetic support with sodium surface doped.

under nitrogen atmosphere. The precursor, likely consisting of a diamine complex (32) of Pd anchored to two oxygens of the support surface, was centrifuged and washed with H_2O (five times), dried in an oven at 353 K, under vacuum for 10 h, then calcined in oxygen at 573 K (0.5°C/min) to eliminate ammonia, and finally reduced in hydrogen for 10 h at 573 K (0.5°C/min).

The other method, producing good metal particle dispersion on low-surface-area supports (35), was already used for the preparation of the natural pumice catalysts (36). It consisted of reacting the hydroxyl groups of pumice with the $Pd(C_3H_5)_2$ complex in pentane, followed by reduction at low temperature. Details of the experimental procedure have been previously described (36).

Methods

Element concentration of the supports and catalysts were obtained by atomic absorption spectrophotometry (AAS) analyses with an accuracy of 10%.

X-ray analysis. The structure of the supports and Pd catalysts was checked with X-ray diffraction measurements performed on a Philips vertical goniometer connected to a highly stabilized generator (Siemens Kristalloflex 805). Nickel-filtered Cu$K\alpha$ radiation was employed and the diffracted beam was monochromatized with a focusing graphite monochromator (Bragg–Brentano geometry). A proportional counter and 0.05° step sizes in 2θ for an accumulated counting time of 100 s per angular abscissa were used. Details for acquisition and calculations were reported previously (36). For palladium content above 0.3 wt% the line broadening of the Pd(111) diffraction peak, according to the Scherrer method, was used to obtain the metal particle sizes. For lower Pd content, the particle diameters were obtained by small angle X-ray scattering (SAXS) analysis following a procedure described in Ref. (36).

Infrared analysis. The FTIR spectra were recorded with a Bruker IFS 5 48 instrument with a resolution of 2 cm^{-1}. The samples were analyzed as thin pellets obtained mixing equivalent amounts of support and KBr and using a pressure of 180 kg cm^{-2}.

Specific surface area and specific pore size volume determination. The microstructural characterization of the supports was carried out with a Carlo Erba Sorptomat 1900 instrument. By the analysis of the adsorption isotherm of nitrogen on the samples cooled in liquid nitrogen, through a fully computerized system, the specific surface areas and the specific pore volumes were calculated. Before measurements the samples were outgassed for 12 h at 523 K to remove water moisture.

Thermal analysis. Thermogravimetric analysis (TGA) and differential thermal analysis (DTA) were performed on a STA 1500 Stanton Redcroft instrument operating in the range 293–1073 K, at a heating rate of 5 K min^{-1}. α-Alumina was used as reference for the TG–DTA analyses.

Density determination. The densities of the solids were determined with the Accupyc 1330 by Micromeritics, with helium gas as probe.

XPS analyses. The X-ray photoelectron analyses were performed with a VG ESCALAB Mk II (Vacuum Generator Ltd., UK) equipped with an aluminum anode as unmonochromatized X-ray source (1486.6 eV) run at 20 mA and 15 kV. Sample charging was constant during the analysis so that the energy shifts could be compensated for by referencing all the spectra to the binding energy of the appropriate component of the C 1*s* signal set at 285.0 eV. For the catalyst, the use of the internal standard Si 2*p* of the corresponding support, previously calibrated with respect to C 1*s* yielded the same binding energy values of the Pd 3*d*, as those obtained with respect to the C 1*s* calibration, ruling out any differential charging effects. The spectra were resolved into their Lorentzian and Gaussian components using a nonlinear least square fitting routine. Binding energies and atomic ratios were obtained according to previously described procedures (20–23). The energy values reported here are the average of two measurements whose reproducibility was ±0.1 eV.

RESULTS AND DISCUSSION

Attempts to decrease or increase the percentage of alkali metal ions in natural pumice, by treatment with HNO_3 of different concentrations and for different times in one case, and by addition of the alkali ions in the second case, produced only minor changes in the alkali metal ion concentration. For this reason a series of amorphous aluminosilicates with similar content of silica and alumina as in natural pumice (37) but with different concentrations of alkali metal ions were prepared. The gel-route synthesis was chosen because of the advantage of a higher homogeneity of the final materials with respect to other classical melting methods (38).

The reactions involved in the preparation procedure are:

(a) hydrolysis of the alkoxides as

$$-M-OR + H_2O \Rightarrow -M-OH + ROH \qquad [1]$$

with $M =$ Si, Al, Na, K followed by

(b) polycondensation as

$$-M-OR + M-OH \Rightarrow -M-O-M- + ROH, \qquad [2]$$

producing a transparent gel. By calcination, the gel turns into a vitreous material containing residual hydroxide groups (30). As seen in Table 1, the transition gel → glass occurs with a large change in density, from 1.4 to 2.4 g/cm^3, indicative of a structure shrinkage. This behavior can be

attributed to a thickening of the −Si−O−*M*−O−Si− network and also to the loss of water, as indicated by the TGA.

According to the literature (29) the amount of water added for the hydrolysis of the alkoxides is crucial for the crystallinity of the product. Usually an excess of water of more than 10 times the required stoichiometric amount leads to some crystallinity in the final material. On the other hand a water quantity just above the stoichiometric may not guarantee the complete hydrolysis process. The procedure *a* using larger amount of water produced final supports with a small percentage of crystallinity (10%) as evidenced by the X-ray diffractograms. Procedure *b* gave completely amorphous materials characterized by the typical diffractogram of an amorphous aluminosilicate (36). The best results, as far as the color and purity of the gel is concerned, are obtained by hydrolyzing the alkoxides immediately after they are mixed together and washing the gel with anhydrous *sec*-BuOH and EtOH before calcination, to eliminate unreacted alkoxides and excess of water.

The calcination temperature and the heating rate affect the specific surface area of the materials (30). As shown in Table 1, a higher calcination temperature and also a slow heating rate produce lower specific surface area. Under the reaction conditions of samples *b*, using a calcination temperature of 973 K with a heating rate of 1.7°C/min, supports of larger surface areas than samples *a*, under the same calcination temperature, are generally obtained. Using a temperature of 1173 K with a slower heating rate of 0.3°C/min produces low surface area supports. In conclusion, the method *b*2 allowed for the reproduction of some of the natural pumice structural characteristics, i.e., amorphicity and low specific surface area, which are of interest in kinetic study since they minimize the effect of heat and mass transfer and moreover they increase the efficiency coefficient of the supported metal (2).

The specific surface areas listed in Table 1 are calculated within the BET (39) model. The adsorption isotherms of the various supports, according to the Brunauer classification, are of the IV type with the hysteresis loop characteristic of mesoporous structure (pore sizes between 2 and 50 nm). Within such range of pore sizes, from the desorption branch of the nitrogen isotherms, the specific pore volumes (Table 1) were also obtained, using the procedure developed by Dollimore and Heal (40) assuming that the pores are cylindrical. Overall, the relation between the specific surface area and the pore volume is such that at higher areas correspond larger volumes. The data relative to $gelsynt_0$ and to the corresponding calcined support $synt_0$ indicate a microstructural change from larger pores, formed during the gel formation and determining a relatively low surface area, to smaller and longer cylindrical pores with a larger surface area and slightly smaller volume, formed after the calcination process.

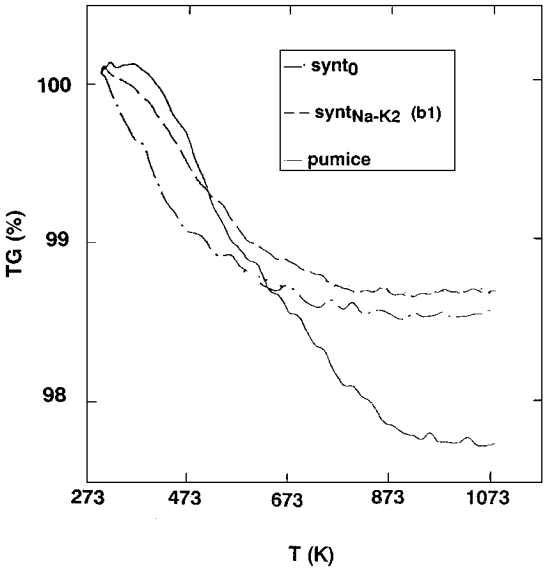

FIG. 1. TG curve of samples, $synt_0$, $synt_{Na\text{-}K_2}$ (*b*1), and pumice.

In Fig. 1 the TGA profiles of selected samples, $synt_0$, $synt_{Na\text{-}K_2}$ (*b*1), and natural pumice are reported. At about 623 K the synthetic supports have lost most of the water, unlike pumice, which seems to retain water up to 873 K. The much higher temperatures involved in the formation of the volcanic pumice may have determined much stronger water bonding (37). The DTA profile for the $gelsynt_0$ and $synt_0$ are shown in Fig. 2. According to previous findings (30), the exothermic peak around 573 K, observed for the $gelsynt_0$ sample, may be attributed to oxidation of residual organic products which are then removed by the calcination treatment as shown from the $synt_0$ DTA profile.

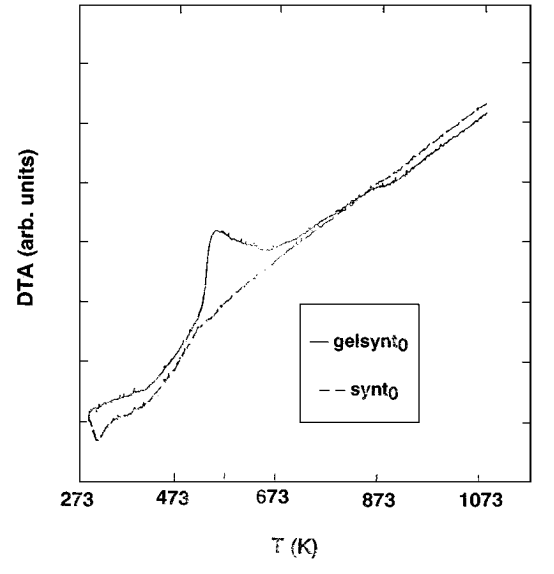

FIG. 2. DTA curve of sample $synt_0$ and precursor $gelsynt_0$.

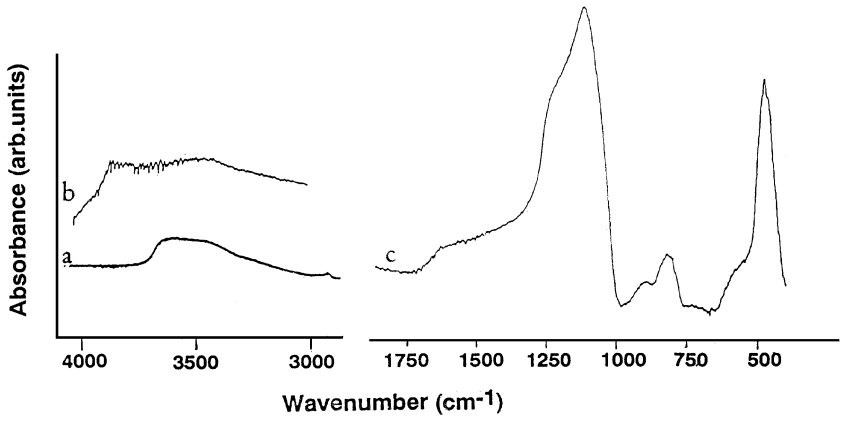

FIG. 3. Enlarged portion of the infrared spectra in the range 4000–3000 cm^{-1} of (a) pumice and (b) *synt*$_0$. (c) IR spectrum in the range 1750–350 cm^{-1} of *synt*$_0$.

The density values are listed in Table 1. All the supports with relatively low area (10–81 m^2/g) have values typical of the skeletal density of an aluminosilicate. Those supports with higher specific surface area are characterized by a low density, in accord with the more porous structure indicated by the larger specific pore volume.

The infrared spectra of the synthetic supports are practically the same, regardless the different amount of alkaline ions and also the preparation procedure, they are characteristic of the aluminosilicates (41, 42). In Fig. 3 the region 4000–3000 cm^{-1} of the pumice and *synt*$_0$ samples and the 300–2000 cm^{-1} range of the *synt*$_0$ are reported. The peaks in the range 380–1300 cm^{-1} are attributed to vibrational modes of the basic structural units constituted by TO_4 tetrahedra (T = Al or Si). The high-frequency region (4000–3000 cm^{-1}) is associated with the OH vibrations. Because of a larger quantity of water retained by the porous supports, it is generally difficult to study the infrared spectrum of such region in air. The most interesting feature is represented by a broad peak in the spectra of the synthetic supports above 3780 cm^{-1}. According to the literature, it can be assigned to an OH group bound to an aluminum in an octahedral environment (43). Such a feature is missing in the IR spectrum of pumice, which as indicated by a previous Al^{27} NMR study contains only aluminum in tetrahedral environment (44).

In Table 2 are listed the most significant XPS binding energies of the support elements, Al 2*p*, Si 2*p*, O 1*s*, Na 1*s*, and K $2p_{3/2}$. For comparison, the data of the natural pumice after the purification treatment are also given (44). The Al 2*p* and Si 2*p* binding energies are characteristic of the aluminosilicates. The sodium and potassium energy values are typical of the (+1) species. The binding energies of the different elements do not change significantly with the alkali concentrations and with the preparation procedure. Differences in the full width half maximum (FWHM) of the peaks may arise from morphological effects. Moreover, within the series of supports prepared with method *a*, the O 1*s* region presents two components; the one at higher binding energy can be attributed to a modified silica oxygen and the other at low energy to an alumina component (44–46). In Fig. 4, a typical spectrum of the O 1*s* of the synthetic support *Na-synt* is shown. The presence of a hydroxide species would be difficult to ascertain since its position would be very close to

TABLE 2

Binding Energies of the Main Elements of the Supports

Supports	Al 2*p*	Si 2*p*	O 1*s*[a] (Si–O$^-$, OH$^-$)	O 1*s* (Al–O$^-$)	Na 1*s*	K $2p_{3/2}$
Pumice	74.7 (2.0)	103.5 (2.2)	533.1 (2.2) (80%)	531.7 (2.2)	1072.7 (2.7)	294.2 (2.3)
Synt$_0$ (*a*)	74.9 (2.3)	103.3 (2.3)	532.7 (2.3) (91%)	531.1 (2.3)		
Synt$_{Na_1}$ (*a*)	74.7 (2.2)	103.1 (2.1)	532.5 (2.2) (90%)	531.4 (2.2)	1072.6 (2.4)	
Synt$_{Na_2}$ (*a*)	74.8 (1.9)	103.1 (2.0)	532.4 (2.1) (83%)	530.9 (2.1)	1072.6 (2.3)	
Synt$_{Na_3}$ (*a*)	74.7 (1.9)	103.2 (2.0)	532.6 (1.9) (81%)	531.2 (1.9)	1072.6 (2.2)	
Synt$_{Na_4}$ (*a*)	74.7 (1.9)	103.2 (2.0)	532.6 (2.0) (73%)	531.5 (2.0)	1072.8 (2.2)	
Na-synt (*a*)	74.2 (2.2)	103.1 (2.2)	532.5 (2.2) (32%)	531.1 (2.2)	1073.1 (2.3)	
Synt$_{Na\text{-}K_1}$ (*b*1)	75.0 (2.3)	103.3 (2.5)	532.7 (2.6) (100%)		1072.6 (2.5)	294.0 (2.4)
Synt$_{Na\text{-}K_2}$ (*b*1)	75.1 (2.2)	103.2 (2.4)	532.6 (2.5) (100%)		1072.8 (2.4)	294.2 (2.1)
Synt$_K$ (*b*2)	75.1 (2.2)	103.3 (2.3)	532.5 (2.5) (100%)			294.4 (2.3)

Note. The precision is estimated as ±0.1 eV. The full widths half maximum (FWHM) (eV) are given in parentheses.

[a] The percentage of this component is given in parentheses.

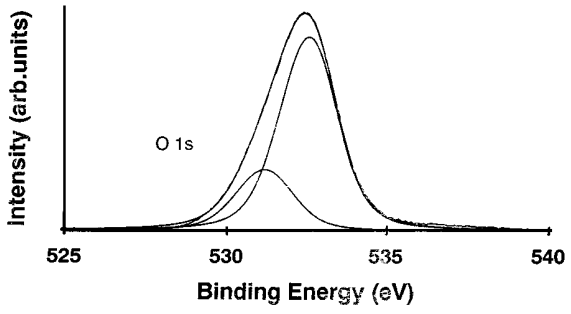

FIG. 4. Experimental and fitted components of the XPS O 1*s* of sample *Na-synt.*

the silica oxygen. However, the decreasing relative intensity of the two components with increasing sodium content is in accordance with a diminished surface Brønsted acidity of the supports; therefore the high-energy peak is likely to contain some hydroxide component. The oxygen peaks relative to the supports prepared by method *b* involving lower calcination temperature have larger FWHM. However, being quite symmetric, they have been fitted with the high-energy component.

The oxygen Auger spectra, O *KLL*, have been collected to obtain further information on the surface chemical state (47) of the different samples. The *KLL* transition of oxygen is in fact an Auger transition of the *KVV* type, i.e., involving the valence levels L_{23}. For this reason, the shape of the peak is dependent on the chemical environment. The Auger spectra of the *Na-synt* is shown in Fig. 5. The two Auger transitions O KL_1L_{23} and O $KL_{23}L_{23}$ are indicated. The spectrum is typical of all the other samples. However, the separation between the two transitions, as given in Table 3, changes. There is a small but steady increase of the separation of the two transitions with increasing sodium content along the *a* sample series. It should be pointed out that, even if the changes are small, they can be considered highly reliable since they are independent on charging and energy referencing processes. Since it has been stated (47) that a decrease of the ionic character of the bond to oxygen produces an increase of the separation of the O *KLL* transitions, it is possible that the addition of the sodium

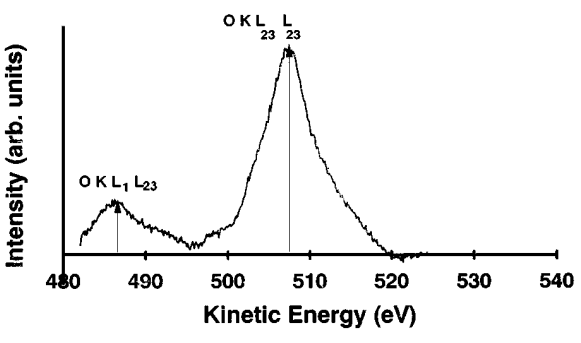

FIG. 5. O *KLL* Auger spectrum of sample *Na-synt.*

TABLE 3

Silicon and Oxygen Modified Auger Parameter and Energy Separation of the Auger Transitions of All Samples

Supports	α' (eV)	KL_1L_{23}–$KL_{23}L_{23}$ (eV)
Pumice	1039.7	21.4
$Synt_0$ (*a*)	1039.6	20.9
$Synt_{Na_1}$ (*a*)	1039.7	21.1
$Synt_{Na_2}$ (*a*)	1039.9	21.2
$Synt_{Na_3}$ (*a*)	1040.0	21.3
$Synt_{Na_4}$ (*a*)	1040.1	21.5
Na-synt (*a*)	1040.2	21.6
$Synt_{Na\text{-}K_1}$ (*b*1)	1039.4	21.0
$Synt_{Na\text{-}K_2}$ (*b*1)	1039.4	20.9

ions, localized near the aluminate ions AlO_2^-, decreases the ionicity of the oxygen bonds to silicon representing the majority of the total oxygen bonds. The modified Auger parameters (48), taken as the kinetic energy of the sharpest Auger line of the O *KLL* plus the binding energy of the most intense O 1*s* component, have been calculated for all the samples and they are reported in Table 3. The values, typical of silica–alumina compounds (48), increase with the sodium content in the *a* sample series. As described before (21), changes in the Auger parameter are related to changes in the extra atomic relaxation energy (R^{ea}) as

$$\Delta\alpha = 2\Delta R^{ea}, \qquad [3]$$

which depends on the polarizability of the whole molecule and therefore on the structural arrangement. The increase of the oxygen parameter with the sodium content suggests an increased polarizability of the electron clouds around the oxygen atoms due to the presence of sodium. The two results, decrease of the ionicity and increase of the polarizability, are complementary and agree with the idea of "group shift" rather than elemental shift (49).

In Table 4 are reported the $(Si/Al)_B$, $(Na/Si)_B$, and $(K/Si)_B$ bulk atomic ratios of all the supports, as determined

TABLE 4

Bulk Atomic Ratios, as Determined by Chemical Analysis, and Corresponding Surface Atomic Ratio, as Determined by XPS Analysis

	$(Si/Al)_B$	$(Si/Al)_{XPS}$	$(Na/Si)_B$	$(Na/Si)_{XPS}$	$(K/Si)_B$	$(K/Si)_{XPS}$
$Synt_0$ (*a*)	5.0	6.4	—	—	—	—
$Synt_{Na_1}$ (*a*)	5.0	5.9	0.01	0.02	—	—
$Synt_{Na_2}$ (*a*)	5.0	5.6	0.04	0.04	—	—
$Synt_{Na_3}$ (*a*)	4.9	4.7	0.09	0.17	—	—
$Synt_{Na_4}$ (*a*)	5.1	4.8	0.15	0.20	—	—
Na-synt (*a*)	4.9	6.8	0.04	0.14	—	—
$Synt_{Na\text{-}K_1}$ (*b*1)	5.0	9.0	0.01	0.01	0.01	0.01
$Synt_{Na\text{-}K_2}$ (*b*1)	5.0	4.6	0.04	0.05	0.03	0.03
$Synt_K$ (*b*2)	5.0	5.0	—	—	0.08	0.08

by chemical analysis, and the corresponding surface atomic ratios, obtained from the XPS measurements. The data in the table are in accord with a homogeneous distribution from the bulk to the surface. The only exception is represented by the $synt_{Na\text{-}K1}$ values, from which an enrichment of silicon at the outermost layers probed by the surface technique seems to occur. A fair agreement exists between the alkali ion to silicon bulk atomic ratios and XPS derived ratios. As expected the support *Na-synt*, which was prepared adding the sodium alkoxide to the already formed $gelsynt_0$, has a large surface segregation of sodium.

Some of the Pd catalysts prepared from the different supports are listed in Table 5 along with the Pd content, the atomic ratio of alkali ions to palladium atoms (R), the dispersion percentage of the metal particle ($\%D$), and the XPS chemical shift of the Pd $3d_{5/2}$ with respect to unsupported metal Pd. As previously established (20) the addition of the metal does not modify the binding energies of the support lines. The Pd 3*d* experimental and fitted photoelectron spectra of the catalyst without sodium, Z_0, and the one with sodium, Na_1, are given in Fig. 6. Detailed studies aimed to determine the effect of metal particle sizes and of increasing sodium concentration have shown that both factors are important in determining the electron density of the Pd particles (22, 23). As confirmed in the present study, the catalyst preparation method does not influence such properties, whereas it does affect the morphology of the particle. With supports of large surface area (>80 m^2/g) both methods of preparation, from ammine or allyl complex, produce good dispersion (23) whereas with the low surface area ($\leq$40 m^2/g) supports, the Pd allyl complex route yields better dispersion. As seen in Table 5, a catalyst containing sodium, Na_1, presents a Pd 3*d* chemical shift of −0.4 eV

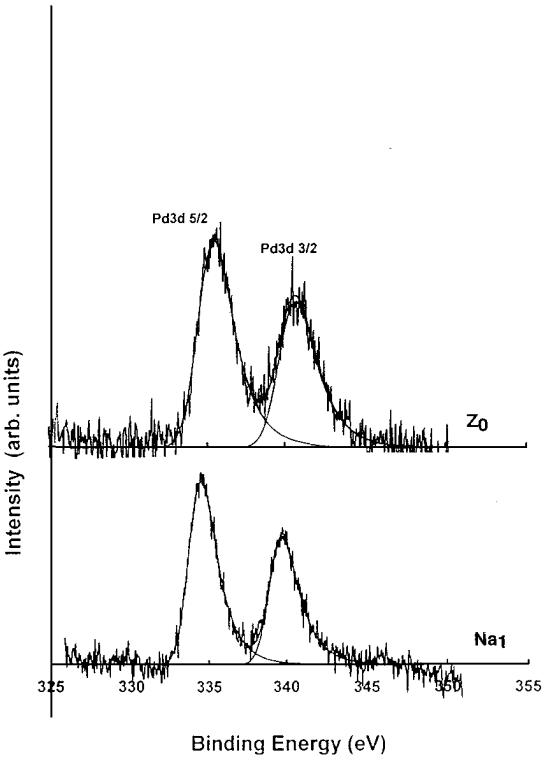

FIG. 6. Experimental and fitted photoelectron spectrum of Pd 3*d* of catalysts Z_0 and Na_1.

differently from the catalyst, Z_0, with the same dispersion but no sodium which does not show any significant chemical shift. Moreover, as already determined for the pumice catalyst (22), there is a limit of sodium concentration, beyond which no further increase in chemical shift is observed. As indicated in Table 5 the addition of potassium does not have significant effect on the photoelectron binding energy of the Pd 3*d*. The difference with sodium could be ascribed to the larger electrostatic field associated with the ion of a smaller radius. As a consequence the dipole (Na^+–O^-) produces a large electron donation to the metallic centers (22).

TABLE 5

Support, Metal Loading, Alkali to Palladium Atomic Ratio Metal Dispersion Percentage, and XPS Chemical Shifts of the Palladium Catalysts

Catalyst	Support	Pd (wt%)	R (Na/Pd)	R (K/Pd)	D (%)[a]	ΔE (Pd $3d_{5/2}$)
Z_0 (ammine)	$Synt_0$ (*a*)	1.2	0	0	39	−0.1
Na_1 (allyl)	$Synt_{Na_2}$ (*a*)	1.4	3.5	0	39	−0.4
Na_4 (ammine)	$Synt_{Na_1}$ (*a*)	0.9	2.1	0	27	−0.5
Na_5 (allyl)	$Synt_{Na_4}$ (*a*)	0.3	68	0	25[b]	−0.5
Na_6 (allyl)	$Synt_{Na_1}$ (*a*)	0.3	6.4	0	18	−0.6
K_0 (allyl)	$Synt_K$ (*b*2)	0.5	0	20	56	−0.1
K_2 (allyl)	$Synt_K$ (*b*2)	0.2	0	64	27[b]	0.1
Pd/*Na-synt* (allyl)	*Na-synt* (*a*)	0.2	22.5	0	12	—

Note. The method of preparation is given in parentheses.

[a] Determined from volume weighted average Pd crystallite diameters obtained by LB analysis of the (111) XRD peak [Ref. (36)].

[b] Determined from SAXS measurements according to a previous procedure [Ref. (36)].

CONCLUSION

Aluminosilicates with variable amounts of sodium and potassium, and with quite homogeneous structure and concentration, were obtained from gels by mixing the appropriate alkoxides in alcoholic solution. As shown with physical techniques and with spectroscopic analysis (XPS and IR), the gel preparation method succeeded in reproducing the most important feature of the natural pumice such as the amorphous structure and the low surface area. With two different procedures of preparation, palladium catalysts with a wide range of atomic ratio of alkali ions to palladium atoms were synthesized. A dependence of the metal particle size from the preparation procedure was found for

the low specific surface area supports. Differently from the sodium ions, determining a negative binding energy shift of the Pd 3*d* level of the catalysts with respect to the unsupported metal Pd, addition of potassium in the support structure does not affect such binding energy.

ACKNOWLEDGMENTS

We thank CNR (Progetto Strategico "Tecnologie Chimiche Innovative"), Ministero dell'Università e della Ricerca Scientifica e Tecnologica (MURST 40%), and Pumex S.p.A. for financial support.

REFERENCES

1. Deganello, G., Duca, D., Liotta, L. F., Martorana, A., and Venezia, A. M., *Gazz. Chim. It.* **124**, 229 (1994).
2. Deganello, G., Duca, D., Martorana, A., Fagherazzi, G., and Benedetti, A., *J. Catal.* **150**, 127 (1994).
3. Deganello, G., Duca, D., Martorana, A., Venezia, A. M., Benedetti, A., and Fagherazzi, G., *J. Catal.* **151**, 125 (1995).
4. Duca, D., Liotta, L. F., and Deganello, G., *J. Catal.* **154**, 69 (1995).
5. Duca, D., Liotta, L. F., and Deganello, G., *Catal. Today* **24**, 15 (1995).
6. Duca, D., Frusteri, F., Parmaliana, A., and Deganello, G., *Appl. Catal. A* **146**, 269 (1996).
7. Boitiaux, J. P., Cosyns, J., and Vasudevan, S., *in* "Preparation of Catalysts. III" (G. Poncelet, P. Grange, and P. A. Jacobs, Eds.), p. 123. Elsevier, Amsterdam, 1983.
8. Boitiaux, J. P., Cosyns, J., and Vasudevan, S., *Appl. Catal.* **15**, 317 (1983).
9. Ryndin, Yu. A., Nosova, L. V., Boronin, A. I., and Chuvilin, A. L., *Appl. Catal.* **42**, 131 (1988).
10. Ryndin, Yu. A., Stenin, M. V., Boronin, A. I., Bukhtiyarov, V. I., and Zaikovskii, V. I., *Appl. Catal.* **54**, 277 (1989).
11. Bertolini, J.-C., Delichere, P., Khanza, B. C., Massardier, J., Noupa, C., and Tardy, B., *Catal. Lett.* **6**, 215 (1990).
12. Tardy, B., Noupa, C., Leclercq, C., Bertolini, J.-C., Hoareau, A., Treilleux, M., Faure, J. P., and Nihoul, G., *J. Catal.* **129**, 1 (1991).
13. Noupa, C., Rousset, J.-L., Tardy, B., and Bertolini, J.-C., *Catal. Lett.* **22**, 197 (1993).
14. Boitiaux, J. P., Cosyns, J., and Vasudevan, S., *Appl. Catal.* **6**, 41 (1983).
15. Hub, S., Hilaire, L., and Touroude, R., *Appl. Catal.* **36**, 307 (1988).
16. Takasu, Y., Unwin, R., Tesche, B., Bradshaw, A. M., and Grunze, *Surf. Sci.* **77**, 219 (1978).
17. Mason, M. G., *Phys. Rev. B* **27**, 748 (1983).
18. Goetz, J., Volpe, M. A., Sica, A. M., Gigola, C. E., and Touroude, R., *J. Catal.* **153**, 86 (1995).
19. Goetz, J., Volpe, M. A., and Touroude, R., *J. Catal.* **164**, 369 (1996).
20. Venezia, A. M., Duca, D., Floriano, M. A., Deganello, G., and Rossi, A., *SIA, Surf. Interface Anal.* **19**, 548 (1992).
21. Venezia, A. M., Duca, D., Floriano, M. A., Deganello, G., and Rossi, A., *SIA, Surf. Interface Anal.* **18**, 619 (1992).
22. Venezia, A. M., Rossi, A., Duca, D., Martorana, A., and Deganello, G., *Appl. Catal. A* **125**, 113 (1995).
23. Venezia, A. M., Rossi, A., Liotta, L. F., Martorana, A., and Deganello, G., *Appl. Catal. A* **147**, 81 (1996).
24. Pitchon, V., Guenin, M., and Praliaud, H., *Appl. Catal.* **63**, 333 (1990).
25. Liotta, L. F., Deganello, G., Delichere, P., Leclercq, C., and Martin, G. A., *J. Catal.* **164**, 334 (1996).
26. Liotta, L. F., Martin, G. A., and Deganello, G., *J. Catal.* **164**, 322 (1996).
27. Liotta, L. F., Venezia, A. M., Martorana, A., and Deganello, G., *J. Catal.* **171**, 177 (1997).
28. Wisseberger, A., and Proskauer, E. S., "Organic Solvents," Vol. VII. Interscience, New York, 1955.
29. Vicarini, M. A., Nicolaon, G. A., and Teichner, S. J., *Bull. Soc. Chim. Franc.*, 1466 (1969), and references therein.
30. Carturan, G., Gottardi, G., and Graziani, M., *J. Non-Cryst. Solids.* **29**, 41 (1978).
31. Carturan, G., and Strukul, G., *J. Catal.* **57**, 516 (1979).
32. Gubitosa, G., Berton, A., Camia, M., and Pernicone, N., *in* "Preparation of Catalysts. III" (G. Poncelet, P. Grange, and P. A. Jacobs, Eds.), p. 431. Elsevier, Amsterdam, 1983.
33. Benesi, H. A., Curtis, R. M., and Studer, H. P., *J. Catal.* **10**, 328 (1968).
34. Fuentes, S., and Figueras, F., *J. Chem. Soc. Faraday Trans.* **74**, 174 (1978).
35. Yermakov, Yu. I., *Catal. Rev.* **13**, 77 (1986).
36. Fagherazzi, G., Benedetti, A., Deganello, G., Duca, D., Martorana, A., and Spoto, G., *J. Catal.* **150**, 117 (1994).
37. Luca, S. F., "La Pomice di Lipari," Techn. Bull., Pumex, Messina, 1986.
38. Mukherjee, S. P., Zaezycki, J., and Traverse, J. P., *J. Mater. Sci.* **11**, 341 (1976).
39. Gregg, S., and Sing, W. K., Adsorption, Surface Area and Porosity. Academic Press, New York, 1982.
40. Dollimore, D., and Heal, G. R., *J. Colloid Interface Sci.* **38**, 109 (1972).
41. Morrow, B. A., *in* "Spectroscopic Characterization of Heterogeneous Catalysts" (J. L. G. Fierro, Ed.), p. A161. Elsevier, Amsterdam, 1990.
42. Yarlagada, P., Lund, C. R. F., and Ruckenstein, E., *J. Catal.* **125**, 421 (1990).
43. Knozinger, K., *in* "Catalysis by Acids and Bases" (B. Imelik, C. Naccache, G. Coudurier, Y. Ben Taarit, and J. C. Vedrine, Eds.), p. 111. Elsevier, Amsterdam, 1985.
44. Venezia, A. M., Floriano, M. A., Deganello, G., and Rossi, A., *SIA, Surf. Interface Anal.* **18**, 532 (1992).
45. Barr, T. L., *J. Vac. Sci. Technol.* **9**, 1793 (1991).
46. Floriano, M. A., Venezia, A. M., Deganello, G., Svensson, E. C., and Root, J. H., *J. Appl. Cryst.* **27**, 271 (1994).
47. Wagner, C. D., Zatko, D. A., and Raymond, R. H., *Anal. Chem.* **52**, 1445 (1980).
48. Wagner, C. D., *Faraday Discuss. Chem. Soc.* **60**, 291 (1975).
49. Barr, T. L., and Lishka, M. A., *J. Am. Chem. Soc.* **108**, 3186 (1986).